Planning of soft-rigid Hybrid arms in Contact with Compliant Environment: application to the transrectal biopsy of the prostate

Eulalie Coevoet, Yinoussa Adagolodjo, Meichun Lin, Christian Duriez, Fanny Ficuciello

Planning of soft-rigid Hybrid arms in Contact with Compliant Environment: application to the transrectal biopsy of the prostate

Eulalie Coevoet[1,2], Yinoussa Adagolodjo[2], Meichun Lin[1,2], Christian Duriez[2], and Fanny Ficuciello[1]

***Abstract*— In this study, a rigid robot is hybridized with a soft part to improve its properties of relative positioning and safe interaction. While the design of the device is quite simple, the kinematics, on the other hand, becomes complex. Pre-operative planning of such a robot is a challenge that is faced in this paper. The clinical context is the automation of transrectal prostate biopsy: a robot is connected to a thin ultrasound (US) probe instrumented with a needle through a flexible silicone part. The procedure consists of: moving the probe near the prostate through the rectum, aligning the probe with identified lesions in the prostate, and shooting the needle to collect tissue samples. In this paper we demonstrate in simulation the feasibility of our methods to solve the planning of the entire procedure. The approach we propose is based on numerical models of both robot and soft tissues, using the Finite Element Method (FEM) to model the soft parts, and a mapping mechanism to propagate the forces and displacements between the soft and rigid models. Finally, we extend the optimization algorithm proposed in previous work for the relative positioning of the hybrid robot on targets in the prostate, as it interacts with the soft tissues. With this formulation we can also set an upper limit to the force the robot is applying on its surroundings, which is particularly critical for the application we study in this paper.**

I. Introduction

Robotics has for decades focused on rigid manipulators, mainly for applications in the industry which require high global precision and force. Soft robotics has provided compliant and safe manipulators to fulfill the need in interaction with fragile environments but generally lacks precision. Soft-rigid hybrid robots could fill the gap and notably offer a precise relative positioning with a safe interaction with fragile environments. The modeling of soft robots is complicated in the general case because of the complex deformations their structure undergoes when subject to actuation and external forces. The problem of their modeling is still actively studied by the community and different approaches have been used such as piecewise constant-curvature assumption [1], and Cosserat theory [2], [3], which are approaches for soft robots with a rod-like shape. The current most accurate models for non-rod-like soft robots are those based on continuum mechanics such as FEM [4], [5], [6]. For articulated robots, existing mathematical formulations are well–established [7]. The modeling of a soft-rigid hybrid arm is then challenging because of the complexity of modeling the soft parts, but also for coupling these soft parts with the rigid articulated system. In this work, we seek to model hybrid robots, composed of an articulated structure connected to soft and rigid parts, and interacting with an environment itself hybrid (rigid and deformable). This modeling is used for the planning of a hybrid robot using the complete inverse kinematics, integrating the articulated, rigid, and soft parts, but also integrating the behavior of the environment and provide relative positioning.

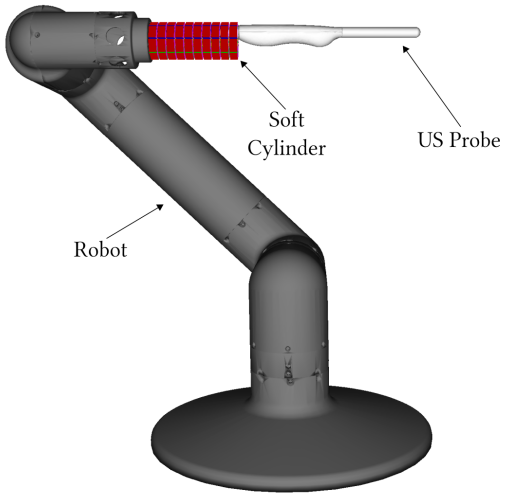

Fig. 1. Numerical model of an articulated soft-rigid hybrid arm. A soft cylinder made of silicone is attached to the robot's end-effector at one end, and a US probe at the other end.

To study the feasibility of our approach, we have conducted numerical experiments in the context of a medical application; the transrectal biopsy of the prostate. During the procedure, a thin US probe is inserted into the patient's rectum close to the prostate to create real-time images of the prostate and retrieve the magnetic resonance imaging (MRI) visible lesions. Then a needle held on the same system and close to the probe is shot into the prostate to collect tissue samples from these lesions. The process

Manuscript received: October, 11, 2021; Revised January, 10, 2022; Accepted February, 1, 2022.

This paper was recommended for publication by Editor C. Laschi upon evaluation of the Associate Editor and Reviewers' comments. This research has been partially funded by the POR FESR 2014–2020 Italian National Program within BARTOLO project (CUP B41C17000090007), by the PNR 2015–2020 Italian National program within PROSCAN Project (CUP E26C18000170005).

[1,2]Eulalie Coevoet and Meichun Lin are with University Federico II Naples, Italy and with Univ. Lille, Inria, CNRS, Centrale Lille, UMR 9189 CRIStAL, F-59000 Lille, France.. eulalie.coevoet@gmail.com

[1]Fanny Ficuciello is with University Federico II Naples, Italy.

[2]Yinoussa Adagolodjo and Christian Duriez are with Univ. Lille, Inria, CNRS, Centrale Lille, UMR 9189 CRIStAL, F-59000 Lille, France. yinoussa.adagolodjo@inria.fr

Digital Object Identifier (DOI): see top of this page.

is often done manually and can be very time consuming, 100.63±(26.24) minutes [8], and tedious for the physician. Indeed, several insertions of needles inside the prostate can cause swelling. This changes the shape of the organ and makes it difficult to identify the region of interest within the image. To overcome the listed problems, robots aided approaches have been proposed in the literature to reduce practitioners fatigue and provide precision and dexterity. These solutions can be divided into two large families, the image-based registration method [9], [10] and the model-based method [11], [12], [13], [14], [15]. In the registration based-method, intra-operative ultrasound image (often poor quality) is improved by registration with the preoperative image MRI [10], [16] in which the area of interest is well defined.

However, it is difficult to extend these methods when the deformations of the tissues are important and it would be necessary here to add the deformations of the soft part of the hybrid robot. To overcome these latter problems, the model-based methods (where finite element [12], [13], [15], [17] method are usually used) use the preoperative images to create the bio-mechanical model and simulate the deformation of the organ. Thus the intra-operative images are used to deform the model in which we have more details on the interested area. The work proposed in this article is part of the last family of methods and extends it to coupling with robot deformations.

Motivations for softness: During the procedure, the patient is awake and can move. For his safety, we place a soft silicone cylinder between the robot and the probe as described in [18] (see Figure 1). Indeed, even if the soft part does not actually come into contact with the patient's body, the introduced passive compliance allows for accommodation of voluntary and involuntary movements of the patient compared with the robot actions, minimizing the interaction forces at the contact. This solution allows the safe use of robotics in this particular application. Another benefit of the soft part is that it allows for a better relative precision.

Contributions: This paper aims at showing the feasibility of planning the relative positioning of a hybrid robot on a deformable environment. To our knowledge, this paper presents the following advances:

- A numerical mechanical model of a hybrid robot contacting the patient's tissues, based on a unified Lagrangian framework, compatible with articulated, rigid or deformable models
- An extension of the inverse kinematics (IK) method for rigid-soft hybrid arms with safe relative positioning on a soft environment
- A feasibility demonstration of preoperative planning for a soft-rigid hybrid robot in the context of transrectal prostate biopsy.

II. Modeling a hybrid robot

One of the challenges in creating a coherent model between articulated, rigid, and deformable parts, is to manage mechanical models described in different spaces. Indeed, the articulated parts are described with a degree of freedom positioned at each joint, the rigid ones with the movement of a frame of reference placed at the center of gravity, and the deformable models (here modeled in FEM) with movements of the nodes of the mesh. In order to allow a mechanical coherence between these models, we rely on a Lagrangian formalism.

This formalism allows us to define hybrid coordinate spaces for the degrees of freedom (DoF). A slave space (called mapped space) is derived by continuous functions to project the mechanics FEM in the coordinate space. After the projection, the system is integrated and solved over time.

A. Coordinate Spaces

To start the hybrid robot modeling, we define the parameterization of the robot's coordinates. Concretely, these DoFs correspond to the motion unknowns that will be solved at each iteration of the planning. We try to avoid kinematic dependencies between the motion parameters. The number of parameters used to describe the model corresponds to the degrees of freedom of the model.

In our case, there are three types of positions:

- reduced coordinates ($\mathbf{q_r}$): used for articulated rigid structures where each joint has its corresponding motion unknown(s). In the case of our robot, we have 5 pivot joints with 1 parameter to describe the position ($\mathbf{q_r} \in \mathbb{R}^5$),
- maximum coordinates ($\mathbf{q_m}$): for the non-articulated rigid parts, the parameterization of the position is given by a reference frame (3 translations, 3 rotations) in $\mathbf{SO}(3)$ space,
- nodal coordinates ($\mathbf{q_n}$): for deformable parts, the geometry is meshed into elements connected by nodes. It is the position of these nodes that describes the shape. However, some nodes of the FEM mesh can be attached to rigid parts. In this case, their position is "slave" to the motion parameters of the rigid body. For deformable parts, the position of the n "free" nodes (not attached to a rigid part) is considered as a degree of freedom (in $\mathbf{q_n} \in \mathbb{R}^{3n}$).

These reduced, maximal, and nodal coordinates can be derived in time to have the position and velocity state of the dynamic system. In the case of a quasi-static calculation, the state is given by the position alone.

B. FEM Slave Space and Projection

Once the coordinates of the robot are defined, slave spaces are derived by mapping functions. Hence, to be able to compute the FEM model of the soft part, we define a space of positions $\mathbf{x}$ of all the nodes of the mesh. As shown in Figure 2, a part of these nodes is related to the reduced coordinates of the rigid robot $\mathbf{q_r}$, another part is related to the maximum coordinates $\mathbf{q_m}$ of the rigid probe, and finally, a part is related to the nodal coordinates $\mathbf{q_n}$ that are not rigidified. We have:

$$\mathbf{x} = \mathcal{M}(\mathbf{q_r}, \mathbf{q_m}, \mathbf{q_n}) \tag{1}$$

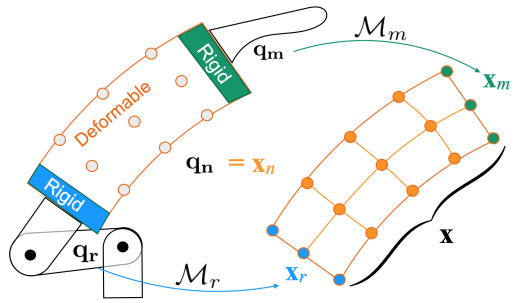

Fig. 2. From coordinate spaces (left) to FEM space (right). The FEM space is obtained using mapping functions.

Where $\mathcal{M}$ is the mapping function. In practice, this mapping function is a gathering of two mappings and one identity:

$$\mathbf{x} = \{\mathbf{x}_r, \mathbf{x}_m, \mathbf{x}_n\} = \{\mathcal{M}_r(\mathbf{q_r}), \mathcal{M}_m(\mathbf{q_m}), \mathbf{q_n}\} \quad (2)$$

This mapping can be derived to obtain the velocities:

$$\dot{\mathbf{x}} = \{\dot{\mathbf{x}}_r, \dot{\mathbf{x}}_m, \dot{\mathbf{x}}_n\} = \left\{ \underbrace{\left(\frac{\partial \mathcal{M}}{\partial \mathbf{q_r}}\right)}_{\mathcal{J}_r} \dot{\mathbf{q}}_\mathbf{r}, \underbrace{\left(\frac{\partial \mathcal{M}}{\partial \mathbf{q_m}}\right)}_{\mathcal{J}_m} \dot{\mathbf{q}}_\mathbf{m}, \dot{\mathbf{q}}_\mathbf{n} \right\} \quad (3)$$

Once the positions $\mathbf{x}$ and velocities $\dot{\mathbf{x}}$ of the FEM nodes are obtained, the internal forces $\mathbf{f}(\mathbf{x}, \dot{\mathbf{x}})$ can be computed in the mapped space. To obtain the equivalent force in coordinate spaces $\boldsymbol{\tau}$, the principle of virtual work is applied, so that the energy remains the same, whatever the space. The transpose of the Jacobians $\mathcal{J}_r$ and $\mathcal{J}_m$ are used:

$$\boldsymbol{\tau} = \begin{bmatrix} \boldsymbol{\tau}_\mathbf{r} \\ \boldsymbol{\tau}_\mathbf{m} \\ \boldsymbol{\tau}_\mathbf{n} \end{bmatrix} = \begin{bmatrix} \mathcal{J}_r^T \\ \mathcal{J}_m^T \\ \mathbb{1}_n^T \end{bmatrix} \mathbf{f}(\mathbf{x}, \dot{\mathbf{x}}) \quad (4)$$

Where $\mathbb{1}_n^T$ is a rectangular identity matrix that selects the nodes that are not rigidified ($\mathbf{x}_n = \mathbb{1}_n^T \mathbf{x}$).

The forces of the FEM are non linear and we use a first order Taylor series expansion to obtain, iteratively, a local linearization:

$$\mathbf{f}(\mathbf{x} + \partial\mathbf{x}, \dot{\mathbf{x}} + \partial\dot{\mathbf{x}}) \approx \mathbf{f}(\mathbf{x}, \dot{\mathbf{x}}) + \mathbf{K}\partial\mathbf{x} + \mathbf{D}\partial\dot{\mathbf{x}} \quad (5)$$

where $\mathbf{K}$ is the tangent stiffness matrix and $\mathbf{D}$ the damping. These matrices are projected in the coordinate spaces using the Jacobians of the mapping to obtain the projected stiffness $\mathbf{K_q}$ and damping $\mathbf{D_q}$ in the coordinate space. For instance, $\mathbf{K_q}$ matrix provides, on the current position of the system, the variation of internal forces of the FEM projected in the coordinate space:

$$\partial\boldsymbol{\tau} = \mathbf{K_q}\partial\mathbf{q} = \begin{bmatrix} \mathcal{J}_r^T\mathbf{K}\mathcal{J}_r & \mathcal{J}_r^T\mathbf{K}\mathcal{J}_m & \mathcal{J}_r^T\mathbf{K}\mathbb{1}_n \\ \mathcal{J}_m^T\mathbf{K}\mathcal{J}_r & \mathcal{J}_m^T\mathbf{K}\mathcal{J}_m & \mathcal{J}_m^T\mathbf{K}\mathbb{1}_n \\ \mathbb{1}_n^T\mathbf{K}\mathcal{J}_r & \mathbb{1}_n^T\mathbf{K}\mathcal{J}_m & \mathbb{1}_n^T\mathbf{K}\mathbb{1}_n \end{bmatrix} \begin{bmatrix} \partial\mathbf{q_r} \\ \partial\mathbf{q_m} \\ \partial\mathbf{q_n} \end{bmatrix} \quad (6)$$

We can identically project the damping matrix but also the mass matrix of the FEM model.

C. Time Integration in the Coordinate Space

Other forces and matrices (like the body mass of the articulated robot) are projected in the same way in the coordinate space. For the time integration, we use a time-stepping implicit scheme (backward Euler) based on a single linearization of the internal forces per step (see [5] for a detailed presentation):

$$\underbrace{\left(\mathbf{M_q} - h\mathbf{D_q} - h^2\mathbf{K_q}\right)}_{\mathbf{A_q}} \Delta\dot{\mathbf{q}} = \underbrace{h\boldsymbol{\tau}(\mathbf{q}, \dot{\mathbf{q}}) + h^2\mathbf{K_q}\dot{\mathbf{q}} + h\boldsymbol{\tau}_{\text{ext}}}_{\mathbf{b_q}} + \mathbf{H}_c(\mathbf{q})^T\boldsymbol{\lambda}_c + \mathbf{H}_a(\mathbf{q})^T\boldsymbol{\lambda}_a \quad (7)$$

where h is the time step, $\mathbf{q}$ the hybrid coordinate positions and $\dot{\mathbf{q}}$ the velocities. $\boldsymbol{\tau}_{\text{ext}}$ gathers the known external forces such as gravity that are projected in the coordinate space. The term $\mathbf{H}_c(\mathbf{q})^T\boldsymbol{\lambda}_c$ represents the contact forces. For these forces, we assume that we know their direction $\mathbf{H}_c(\mathbf{q})$ but not their intensity $\boldsymbol{\lambda}_c$. Same for the $\mathbf{H}_a(\mathbf{q})^T\boldsymbol{\lambda}_a$ which represents the actuator forces. Putting them in Lagrange multiplier form is useful for the following in section IV.

Once we have solved $\Delta\dot{\mathbf{q}}$, we can update the velocities,

$$\dot{\mathbf{q}} \leftarrow \dot{\mathbf{q}} + \Delta\dot{\mathbf{q}}, \quad (8)$$

followed by the update of the positions,

$$\mathbf{q} \leftarrow \mathbf{q} + h\dot{\mathbf{q}}. \quad (9)$$

We can then update the position $\mathbf{x}$ of the FEM nodes using the mapping $\mathcal{M}(\mathbf{q})$. The simulated deformations of the cylinder can be seen on Figure 3.

III. Modeling the Organs of the Pelvic Area

To model the pelvic area of the patient, we start from a set of 3D MRI images (see left image of Figure 4). The connections and interactions between the organs are complex, and very difficult to model with exactness. Instead, we propose to approximate these connections, and how the motion of an organ or bone influences the surrounding tissues, by using a reduced model based on a mapping mechanism on a 3D FEM grid. We also model the contact interaction with the robot.

A. Reduced Model of the Organs

The reduced model is obtained by projection. The body is modeled as a cuboid with a 3D grid which matches the size of the MRI. The organ and bone models are then mapped to the global grid (see right image of Figure 4) using barycentric weight matrices. $\mathbf{p}$ represents the coordinates of the grids and are the degree of freedom. We define a barycentric mapping $\mathcal{B}$ that drives any mapped nodes on this grid, in particular the nodes $\mathbf{x}$ of FEM models that represents the anatomical structures, $\mathbf{x} = \mathcal{B}\mathbf{p}$. As the mapping is linear, the Jacobian of this mapping is constant. Like in the previous section, the forces and displacements of each organ are propagated to its surroundings through the global grid using the transposed Jacobian. Note that we use a FEM-based image warping method, similar to what is proposed in [19], to visualize the deformations of the area on the MRI images when the robot

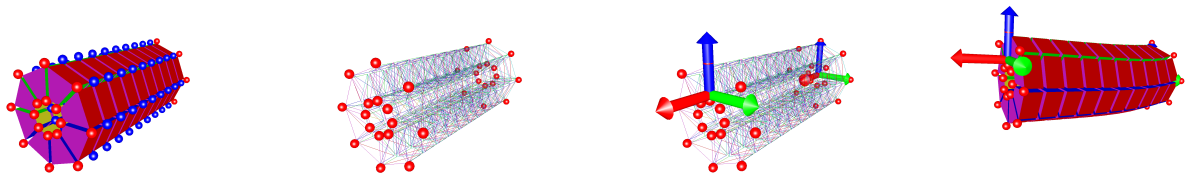

Fig. 3. Each extremity of the soft cylinder is rigidified to attach the robot's end-effector and the probe. From left to right: 1) hexahedral FEM volume mesh of the cylinder, with the FEM nodes (blue spheres), and the rigidified nodes (red spheres), 2) wire-frame view of the hexahedral mesh showing the rigidified nodes at both extremities, 3) the two rigid frames (one for each extremity) followed by the rigidified nodes, and 4) view of the deformed cylinder.

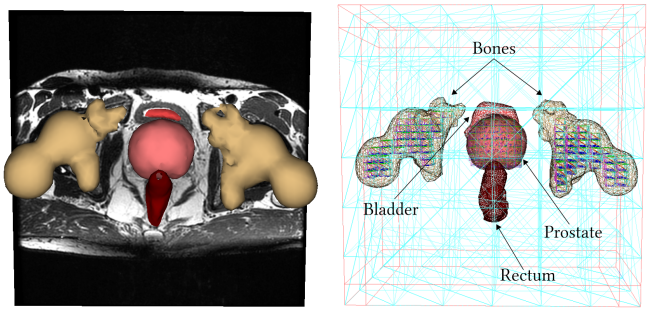

Fig. 4. The soft tissues and bones are extracted from an MRI of the patient. Left: one image of the 3D MRI images set, with the surface meshes of the rectum, prostate, bladder, and bones. Right: the deformable grid used to model the tissues connections and interactions (in wire-frame). The red boxes select the FEM nodes attached with stiff springs.

manipulates the probe in the rectum. Because the patient is supposedly steady during the intervention, we hold the cuboid by selecting FEM nodes on four of its sides and attach them using stiff springs, leaving the inside of the grid free to move.

We use the co-rotational FEM model to model the elasticity of the organs, with a low Young's modulus set to 5 kPa and the Poisson's ratio set to 0. Note that the global grid is coarse, which adds an artificial rigidity to the soft volume. We extract the mesh surfaces of the prostate, rectum, bladder, and bones from the MRI images using the Insight Toolkit (ITK). These triangle meshes are then used in the simulation for visualization and collision processing. In comparison to the rectum and bladder, the prostate is considered as more rigid. To take this difference into account, we use a hexahedral representation of the prostate, which we generate from the surface mesh, and map this FEM volume to the global grid. The Young's modulus of the prostate is set to 1 kPa, which is added to the 5 kPa of the grid through the mapping. A similar approach is used to rigidify parts of the grid that correspond to the bones (1 GPa).

We use the same time integration scheme as for the robot, leading to a similar system of equations:

$$\mathbf{A}_p \Delta\dot{\mathbf{p}} = \mathbf{b}_p + \mathbf{H}_c(\mathbf{p})^T \boldsymbol{\lambda}_c \tag{10}$$

with the matrix $\mathbf{A}_p$ that represents the projection of the FEM matrices in the reduced space of the grid $\mathbf{A}_p = \mathcal{B}^T(\mathbf{M} - h\mathbf{D} - h^2\mathbf{K})\mathcal{B}$ where $\mathbf{M}$, $\mathbf{D}$ and $\mathbf{K}$ are the mass, damping and stiffness matrices computed on FEM model of the organs. The same projection is used to compute $\mathbf{b}_p$. $\mathbf{H}_c(\mathbf{p})^T\boldsymbol{\lambda}_c$ represents the contact forces projected on the coordinate system of the grid.

B. Contact with the Robot in Direct Kinematics

To handle the collision between the probe and the rectum while we actuate the arm, we formulate a constraint problem using the Lagrange multipliers. By formulating these constraints, we open new spaces in which the behavior laws related to the constraints are defined. These spaces are also "mapped" on the coordinates of the mechanical systems (hybrid robot and organs). We introduce Lagrange multipliers as new variables in the contact space and in the actuation space to define non-continuous laws (complementarity constraints for contact and actuator stops).

In this work we only consider sliding contacts (i.e. without friction) using Signorini's complementarity conditions [20][21]. Indeed, the tips of the probes usually have special low-friction finish to aid in the ease of placement and patient comfort.

Let us consider the contacts distance between the probe and the rectum $\boldsymbol{\delta}_c$ at the beginning of the step and $\Delta\boldsymbol{\delta}_c$ its variation over the step. This distance and the contact forces $\boldsymbol{\lambda}_c$ need to follow the Signorini's law [21]:

$$0 \leq \boldsymbol{\lambda}_c \perp \boldsymbol{\delta}_c + \Delta\boldsymbol{\delta}_c \geq 0$$

For the joints actuator, we use Lagrange multipliers. Their dual value, $\boldsymbol{\lambda}_a$, represents the angles of rotation of the joints. When using the robot with direct kinematics, the variation of the angle over a time iteration step $\Delta\boldsymbol{\lambda}_a$ is known.

The coupling between the models of the robot and the tissues is then given by:

$$\begin{bmatrix} \mathbf{A_q} & 0 & h\mathbf{H}_c(\mathbf{q})^T & h\mathbf{H}_a(\mathbf{q})^T \\ 0 & \mathbf{A_p} & h\mathbf{H}_c(\mathbf{p})^T & 0 \\ h\mathbf{H}_c(\mathbf{q}) & h\mathbf{H}_c(\mathbf{p}) & 0 & 0 \\ h\mathbf{H}_a(\mathbf{q}) & 0 & 0 & 0 \end{bmatrix} \begin{bmatrix} \Delta\dot{\mathbf{q}} \\ \Delta\dot{\mathbf{p}} \\ \boldsymbol{\lambda}_c \\ \boldsymbol{\lambda}_a \end{bmatrix} = \begin{bmatrix} \mathbf{b}_p \\ \mathbf{b}_q \\ \Delta\boldsymbol{\delta}_c \\ \Delta\boldsymbol{\delta}_a \end{bmatrix} \tag{11}$$

If we know the values $\Delta\boldsymbol{\delta}_a$ for the joints, the system to solve is a mixed problem with complementarity constraints (MCP), where the unknown are the velocities change $\Delta\dot{\mathbf{q}}$ and $\Delta\dot{\mathbf{p}}$, the contact force intensities $\boldsymbol{\lambda}_c$ on which there are complementarity constraints and actuation efforts $\boldsymbol{\lambda}_a$ on which there are equality constraints. We solve this problem using a Gauss-Seidel algorithm [21].

IV. Inverse Kinematics and Planning

The planning presented in this paper uses an algorithm presented in [5], [22] to have the IK of the hybrid robot in contact with a deformable environment. In this section we present the key features of the methods and demonstrate its use for planning, but we invite the reader to refer to the two papers cited above for a detailed presentation.

A. Compliance projection and Probe Steering

We define a new space in which $\boldsymbol{\delta}_e$ is the distance between the effector (the probe tip) and a target point. Depending on the case, $\boldsymbol{\delta}_e \in SO(3)$ or $\boldsymbol{\delta}_e \in R^3$ (see section IV-C) $\boldsymbol{\delta}_e$ is mapped from $\mathbf{q_m}$, so more generally from $\mathbf{q}$ for the robot, and the target can also be mapped on the FEM of soft tissue ($\boldsymbol{\delta}_e(\mathbf{q}, \mathbf{p})$). We define the constraint matrix $\mathbf{H}_e(\mathbf{q}) = \frac{\partial \boldsymbol{\delta}_e}{\partial \mathbf{q}}$ and $\mathbf{H}_e(\mathbf{p}) = \frac{\partial \boldsymbol{\delta}_e}{\partial \mathbf{p}}$. When the target point is defined in global space (not on the soft tissue), $\mathbf{H}_e(\mathbf{p}) = 0$.

The corresponding multipliers $\boldsymbol{\lambda}_e$ are set to zero as we do not want to apply any forces directly on the effector. We formulate the problem as an optimization program, which is one of the most popular approaches in rigid robotics. Indeed, this formulation allows for instance to easily handle singularity problems and joint limits.

We can gather the constraint matrices by mechanical system:

$$\mathbf{H}_q = \begin{bmatrix} \mathbf{H}_c(\mathbf{q}) \\ \mathbf{H}_a(\mathbf{q}) \\ \mathbf{H}_e(\mathbf{q}) \end{bmatrix} \; ; \; \mathbf{H}_p = \begin{bmatrix} \mathbf{H}_c(\mathbf{p}) \\ 0 \\ \mathbf{H}_e(\mathbf{p}) \end{bmatrix} \tag{12}$$

To solve the optimization, we use the Schur complement of the matrix in equation (11) (with, additionally, the effector constraints). $\mathbf{W} = h\mathbf{H}_q^T \mathbf{A}_\mathbf{q}^{-1} \mathbf{H}_q + h\mathbf{H}_p^T \mathbf{A}_\mathbf{p}^{-1} \mathbf{H}_p$, which is also a popular approach, to solve the optimization in the reduced space of the constraints (effector, actuation and contacts). The computation of this reduced space is also a projection, but using the inverse matrices $\mathbf{A}_\mathbf{q}^{-1}$ and $\mathbf{A}_\mathbf{p}^{-1}$ that are homogeneous to compliance.

Note that the matrix $\mathbf{W}$ provides the mechanical coupling between the actuation of the arm, the position and orientation of the probe tip, and the contact with the rectum's wall. We solve the singularity problems in the actuation of the arm by adding to the objective of the optimization, an expression of the actuators' energy $\epsilon\mathbf{E}$ (with ϵ chosen sufficiently small to keep a good accuracy on the effector motion). The optimization program is then a quadratic program with complementarity constraints (QPCC),

$$\begin{aligned} & \min_{\boldsymbol{\lambda}}(||\boldsymbol{\delta}_e||^2 + \epsilon\mathbf{E}) \\ s.t: & \\ & 0 \leq \boldsymbol{\lambda}_c \perp \boldsymbol{\delta}_c \geq 0 \\ & \mathbf{l}_{min} \leq \Delta\boldsymbol{\delta}_a + \boldsymbol{\delta}_a^0 = \mathbf{W}_a\boldsymbol{\lambda} + \boldsymbol{\delta}_a^0 \leq \mathbf{l}_{max} \end{aligned} \tag{13}$$

with $\boldsymbol{\delta}_e = \mathbf{W}_e\boldsymbol{\lambda} + \boldsymbol{\delta}_e^0$ the shift between the position and orientation of the probe tip, and its target, where $\mathbf{W}_e$ selects the lines of the matrix $\mathbf{W}$ corresponding to the effector, and $\boldsymbol{\delta}_e^0$ contains the initial[1] distance and orientation to the target and $\boldsymbol{\delta}_a^0$ the initial position of the actuators. The limits of the joints, such as stops, are gathered in the vectors $\mathbf{l}_{min}$ and $\mathbf{l}_{max}$. We can also use these limits to set a maximum velocity to each joint.

We solve this QPCC using the iterative approach we present in [22]; we use the disjunctive structure of the complementarity constraints to formulate the QPCC as a series of the quadratic program (QP). Each QP resolution being a component of the global problem. We use the solvers provided in the qpOASES library [23] to solve each QP. Note that by using an optimization program, we always provide an optimal configuration for the robot, even if the objective is not in the working space.

B. Contact Force Limit

Another interesting aspect of this formulation is that we can limit the global force the probe tip is applying on the rectum (and the prostate) by adding the following constraint to the system of equations (13),

$$\mathbb{1}_c^T \boldsymbol{\lambda} < l_{max}, \tag{14}$$

with $\mathbb{1}_c \in \mathbb{R}^k$ a column matrix of ones at the lines corresponding to the contacts, and zeros elsewhere. This constraint sets a maximum to the sum of the contact forces, limiting the force the probe is applying on the organs, which is critical for the safety and comfort of the patient. Note that the limit l_{max} can be found by experiments with the simulation. Similarly we can also set a strict minimum to this sum (usually $l_{min} = 0$) which guarantees that the probe stays in contact with the rectum's wall.

C. Needle Insertion Planning

The procedure can be split into three steps. For the first step, we solve the IK of the hybrid arm, so that the probe reaches the rectum's wall. We solve this problem by formulating an optimization program. During this step the objective of the optimization is to minimize the distance between the probe and a predefined trajectory (in position and orientation). In that case $\boldsymbol{\delta}_e \in \mathbf{SO(3)}$ depends only on $\mathbf{q}$.

For the second step of the planning, we align the probe direction with a target region in the prostate. The objective of the optimization is a $\mathbb{R}^3$ distance. In such case $\boldsymbol{\delta}_e$ depends on both $\mathbf{q}$ and $\mathbf{p}$. Finally, once the configuration of the robot is valid, as a third step, we verify that we can shoot the needle at the target to collect the tissue sample.

To collect the tissue sample in the prostate, the needle is inserted at high speed (i.e. 6 m.s^{-1}) on a straight trajectory. For this last step of the procedure the arm has a fixed configuration, and a forward simulation is performed to direct the tip of the needle to the destination. We will not dwell on this aspect of the simulation since the high insertion speed makes both needle and tissue deformation negligible [24]. But the approach would be compatible with already proposed needle-tissue interaction model, such as [25], in our previous works.

[1] at the beginning of the step

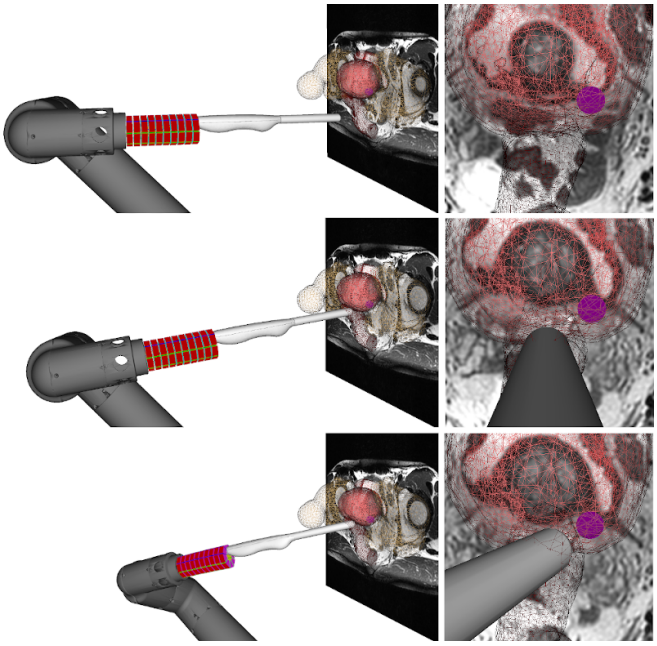

Fig. 5. Two steps planning of the procedure. The organs surface meshes are displayed in wire-frame to show the probe and a target region inside the rectum and prostate. Top: initial configuration of the robot and the patient. Middle: results of the optimization of the first step of the procedure; insertion of the probe into the rectum. Bottom: results of the optimization of the second step of the procedure; alignment of the probe with a target in the prostate (purple sphere).

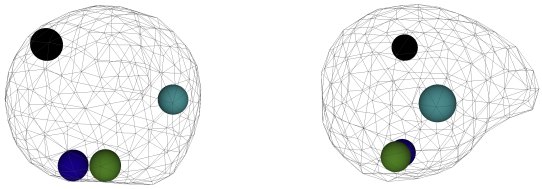

Fig. 6. Two different views of the surface mesh of the prostate in wire-frame, with spheres representing target regions defined by a physician.

V. Experiments

In this section we present the results we obtain in simulation. In the current implementation, each step of the procedure is solved in a different simulation. In the first step, we solve the IK of the robot to insert the probe into the rectum (global positioning while limiting contact forces). When in place, we can start the second step where we solve the probe alignment with some target positioned on the prostate (local positioning while limiting contact forces). This second step which is the most complex and shows the interest of the method.

Note that the only difference between the two planning steps is the objective of the inverse problem. Figure 5 shows these two planning steps.

For the local positioning step, there are usually multiple regions in the prostate where the physician can collect a tissue sample. These regions can be represented by spheres of 0.5 cm radius, and are generally located near the surface

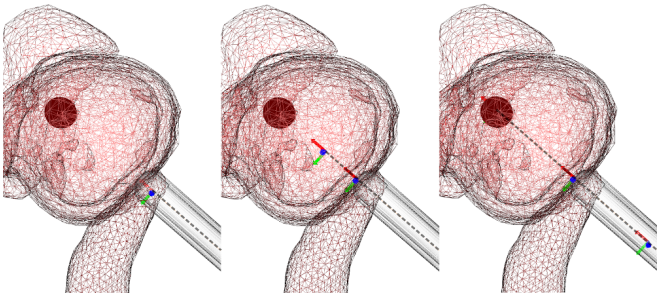

Fig. 7. Needle insertion simulation. The frames represent the beam DoFs. The needle is highlighted by a dashed gray line. One Dof is maintained on the prostate surface, at the entry point of the beam. The red sphere represents the target region.

of the prostate (see Figure 6). After the selection of one region, the objective is set to minimize the distance between the center of the target region and its projection on the probe longitudinal axis. Then the planning automatically finds the actuators motion on the rigid robot to optimize this alignment, while keeping safe contact forces.

After this second planning phase, at each region, we can simulate the needle insertion into the prostate (see Figure 7).

The rigid arm has five active joints, the soft cylinder has 176 FEM nodes (deformable and rigidified nodes), and the 3D grid representing the body has 196 FEM nodes. The simulation runs at an average of 53 ms per frame, with an average of 73 constraints, including the joint forces, effector constraints, and contact forces. We performed the timing on a laptop with an Intel Core i7-9750H CPU at 2.60 GHz $\times$ 12, 16 GB of DDR4 system memory. This performance suggests the possibility of re-planning online, or even using this optimization in a closed loop.

In Figure 8 we show the alignment's results we obtain for the four target regions shown in Figure 6, that are defined by a physician. The error is always zero, meaning that the needle is always successfully shot inside the targeted region. Generally, the patient lies on an operating bed with a lifting mechanism. By moving the bed up and down, we can place the target region in the working space of the robot. This suitable position can also be found by trials using the simulation. For instance, three of the targets in Figure 6 were solved using the same position for the bed, while the fourth one, i.e. the black sphere in Figure 6, required to move the bed in a higher position. This shows the relevance of a pre-operative planning which would allow to anticipate this kind of situation.

Finally, the simulation can also be used for design purposes. In Figure 9 we show the results of the alignment task with different Young's modulus for the soft cylinder; 18 MPa, 0.8 MPa, and 0.08 MPa. The algorithm successfully aligns the probe in the three cases, and we can see how this parameter changes the deformations of the cylinder. The softness of the cylinder plays an important role for the safety of the patient. However it also impacts the workspace of the robot as this softness limit the forces the probe is able to apply in the rectum.

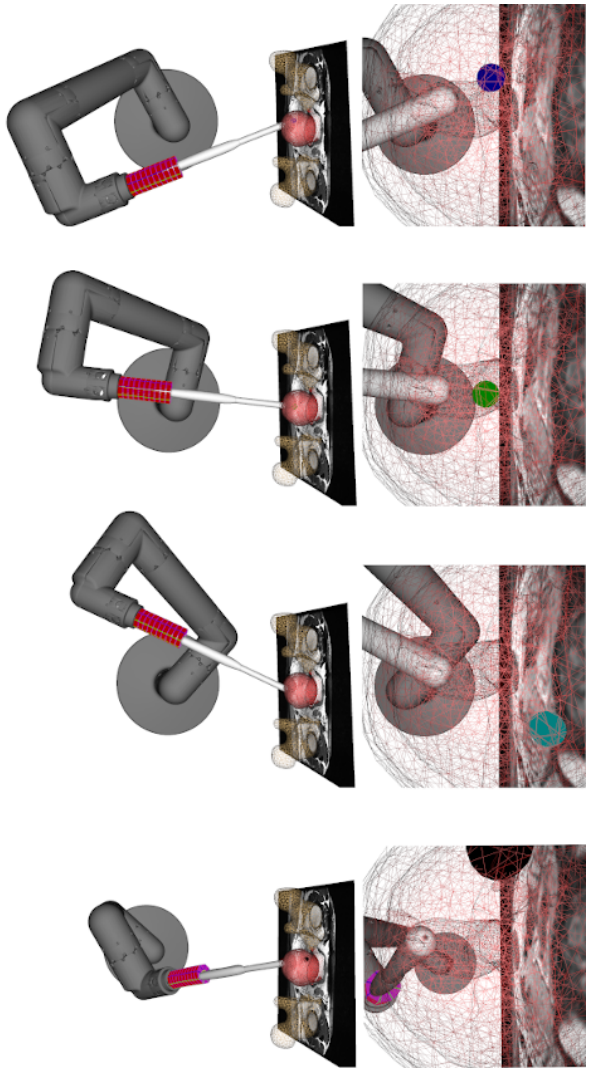

Fig. 8. Results of the alignment step for the four target regions of Figure 6.

VI. Discussion and Future Work

In this paper we focus on the challenges of planning and modeling of soft-rigid hybrid arms in a deformable environment. We propose a methodology and present some validations in simulation. Although the geometry of the soft part used for the application presented in this paper is quite simple (i.e. a cylinder), the approach we propose is generic and allows us to model arms coupled with different and more complex geometries, such as soft fingers and tentacles.

Future work will address online registration to go one step further in the achievement of a real system. For the biopsy of the prostate, because the MRI images are taken prior the intervention and do not match the actual configuration of the organs, one technique is to co-register the MRI with the real-time ultrasound images collected by the probe [26]. In order to match the simulation with the reality, and because it is hard to model with exactness the mechanical behavior of the biological tissues, we want to investigate the registration of the simulated organs with respect to the fused MRI and ultrasound images. Some artificial registration forces, based on the differences between the fused and warped MRI images, can be determined in a different simulation running concurrently, and then applied to the 3D FEM grid representing the organs. As presented in section IV-B, we can add a limit to the total contact forces the probe is applying on the rectum. If a force sensor in mounted on the real robot, this maximum force can be adjusted consequently.

VII. Conclusion

We have proposed a methodology to model and solve the IK of soft-rigid hybrid arms in a deformable environment. The method is generic as it can work with different designs of combined soft, rigid, and articulated parts. It is based on the mapping mechanism of SOFA to couple soft and rigid components, the FEM to model the deformable objects, and an optimization program to solve the IK. We have demonstrated in the simulation the feasibility of the approach of a specific context; the automation of the transrectal biopsy of the prostate. We are able to solve the planning of the entire procedure with simulations that run in real-time. In addition, we can constrain the robot to limit the force it applies on the organs at the contact location, which is critical for the safety and comfort of the patient. We have succeeded in solving the planning on multiple scenarios which were defined by a physician. Finally, also with the use of the mapping mechanism of SOFA, we have presented an approach to simplify the simulation of the connections and interactions between the organs.

References

[1] C. Della Santina, A. Bicchi, and D. Rus, "On an improved state parametrization for soft robots with piecewise constant curvature and its use in model based control," IEEE Robotics and Automation Letters, vol. 5, no. 2, pp. 1001–1008, 2020.

[2] D. C. Rucker, B. A. Jones, and R. J. Webster III, "A geometrically exact model for externally loaded concentric-tube continuum robots," IEEE Transactions on Robotics, vol. 26, no. 5, pp. 769–780, 2010.

[3] D. Trivedi, A. Lotfi, and C. D. Rahn, "Geometrically exact models for soft robotic manipulators," IEEE Transactions on Robotics, vol. 24, no. 4, pp. 773–780, 2008.

[4] S. Grazioso, G. Di Gironimo, L. Rosati, and B. Siciliano, "Modeling and simulation of hybrid soft robots using finite element methods: Brief overview and benefits," in International Symposium on Advances in Robot Kinematics. Springer, 2020, pp. 335–340.

[5] E. Coevoet, T. Morales-Bieze, F. Largilliere, Z. Zhang, M. Thieffry, M. Sanz-Lopez, B. Carrez, D. Marchal, O. Goury, J. Dequidt, and C. Duriez, "Software toolkit for modeling, simulation, and control of soft robots," Advanced Robotics, vol. 31, no. 22, pp. 1208–1224, 2017.

[6] J. M. Bern, P. Banzet, R. Poranne, and S. Coros, "Trajectory optimization for cable-driven soft robot locomotion." in Robotics: Science and Systems, vol. 1, no. 3, 2019.

[7] B. Siciliano and O. Khatib, Springer handbook of robotics. Springer, vol. 200.

[8] G. Tilak, "Comparison of robotic and manual needle-guide templates in mri-guided transperineal prostate biopsy," Ph.D. dissertation, 2017.

[9] D. Stoianovici, D. Song, D. Petrisor, D. Ursu, D. Mazilu, M. Mutener, M. Schar, and A. Patriciu, ""mri stealth" robot for prostate interventions," Minimally Invasive Therapy & Allied Technologies, vol. 16, no. 4, pp. 241–248, 2007. [Online]. Available: https://doi.org/10.1080/13645700701520735

[10] N. Hungr, M. Baumann, J.-A. Long, and J. Troccaz, "A 3-d ultrasound robotic prostate brachytherapy system with prostate motion tracking," IEEE Transactions on Robotics, vol. 28, no. 6, pp. 1382–1397, 2012.

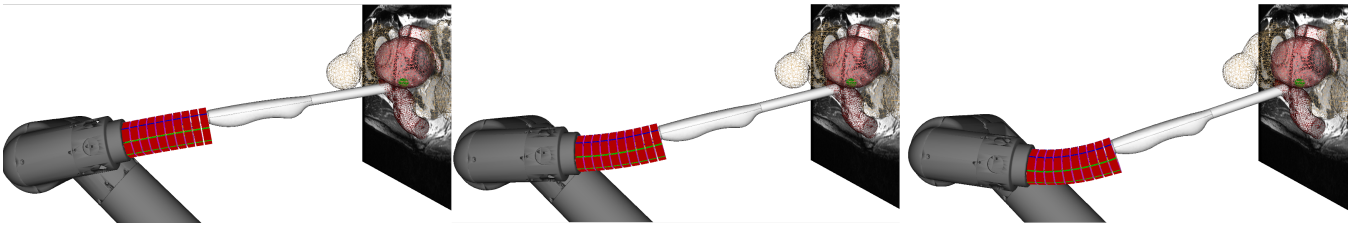

Fig. 9. Results of the alignment step with three different Young's modulus for the soft cylinder. From left to right 18 MPa, 0.8 MPa, and 0.08 MPa. The target region is the same in the four cases, and the algorithm succeeds in solving the tasks.

[11] M.-A. Vitrani, J. Troccaz, A.-S. Silvent, S. Selmi, J. Sarrazin, D. Reversat, E. Promayon, C. Poquet, P. Mozer, G. Morel, G. Fiard, A. Moreau-Gaudry, A. Leroy, M. Janier, and M. Baumann, "PROSBOT – Model and image controlled prostatic robot," Innovation and Research in BioMedical engineering, vol. 36, no. 2, pp. 118–125, Mar. 2015. [Online]. Available: https://hal.archives-ouvertes.fr/hal-02347634

[12] J. R. Crouch, S. M. Pizer, E. L. Chaney, Y.-C. Hu, G. S. Mageras, and M. Zaider, "Automated finite-element analysis for deformable registration of prostate images," IEEE Transactions on Medical Imaging, vol. 26, no. 10, pp. 1379–1390, 2007.

[13] R. Alterovitz, K. Goldberg, J. Pouliot, I.-C. Hsu, Y. Kim, S. M. Noworolski, and J. Kurhanewicz, "Registration of mr prostate images with biomechanical modeling and nonlinear parameter estimation." Medical physics, vol. 33 2, pp. 446–54, 2006.

[14] M. Loughlin, I. Carlbom, C. Busch, T. Douglas, L. Egevad, H. Frimmel, M. Norberg, I. Sesterhenn, and J. M. Frogge, "Three-dimensional modeling of biopsy protocols for localized prostate cancer," Computerized Medical Imaging and Graphics, vol. 22, no. 3, pp. 229–238, 1998. [Online]. Available: https://www.sciencedirect.com/science/article/pii/S0895611198000196

[15] Y. Fu, T. Wang, Y. Lei, P. Patel, A. B. Jani, W. J. Curran, T. Liu, and X. Yang, "Deformable mr-cbct prostate registration using biomechanically constrained deep learning networks," Medical physics, vol. 48, no. 1, pp. 253–263, Jan 2021, 33164219[pmid]. [Online]. Available: https://pubmed.ncbi.nlm.nih.gov/33164219

[16] S.-Y. Selmi, E. Promayon, and J. Troccaz, "Hybrid 2D–3D ultrasound registration for navigated prostate biopsy," International Journal of Computer Assisted Radiology and Surgery, vol. 13, no. 7, pp. 987–995, July 2018. [Online]. Available: https://hal.archives-ouvertes.fr/hal-01739427

[17] Y. Adagolodjo, N. Golse, E. Vibert, M. De Mathelin, S. Cotin, and H. Courtecuisse, "Marker-based Registration for Large Deformations -Application to Open Liver Surgery," in ICRA 2018 - International Conference on Robotics and Automation, Brisbane, Australia, May 2018. [Online]. Available: https://hal.inria.fr/hal-01792837

[18] C. Pecorella, A. Cirillo, B. Siciliano, A. Iele, A. Ricciardi, M. Consales, A. Cusano, M. Capece, G. Celentano, R. La Rocca, et al., "Robot-aided prostate cancer diagnosis with fiber optic sensing: A validation study on phantoms and ex-vivo tissues," Uro, vol. 1, no. 4, pp. 245–253, 2021.

[19] H. Zhong, T. Peters, and J. V. Siebers, "Fem-based evaluation of deformable image registration for radiation therapy," Physics in Medicine & Biology, vol. 52, no. 16, p. 4721, 2007.

[20] A. Signorini, "Questioni di elasticità non linearizzata e semilinearizzata," Rend. Mat. Appl, vol. 18, no. 5, pp. 95–139, 1959.

[21] C. Duriez, F. Dubois, A. Kheddar, and C. Andriot, "Realistic Haptic Rendering of Interacting Deformable Objects in Virtual Environments," IEEE Transactions on Visualization and Computer Graphics, vol. 12, no. 1, pp. 36–47, 2006. [Online]. Available: https://hal.archives-ouvertes.fr/hal-00269404

[22] E. Coevoet, A. Escande, and C. Duriez, "Optimization-based inverse model of soft robots with contact handling," IEEE Robotics and Automation Letters, vol. 2, no. 3, pp. 1413–1419, 2017.

[23] H. J. Ferreau, C. Kirches, A. Potschka, H. G. Bock, and M. Diehl, "qpoases: A parametric active-set algorithm for quadratic programming," Mathematical Programming Computation, vol. 6, no. 4, pp. 327–363, 2014.

[24] M. Mahvash and P. Dupont, "Fast needle insertion to minimize tissue deformation and damage," IEEE International Conference on Robotics and Automation : ICRA : [proceedings] IEEE International Conference on Robotics and Automation, vol. 2009, pp. 3097–3102, 07 2009.

[25] Y. Adagolodjo, L. Goffin, M. de Mathelin, and H. Courtecuisse, "Inverse real-time finite element simulation for robotic control of flexible needle insertion in deformable tissues," in 2016 IEEE/RSJ International Conference on Intelligent Robots and Systems (IROS), 2016, pp. 2717–2722.

[26] J. K. Logan, S. Rais-Bahrami, B. Turkbey, A. Gomella, H. Amalou, P. L. Choyke, B. J. Wood, and P. A. Pinto, "Current status of mri and ultrasound fusion software platforms for guidance of prostate biopsies," BJU international, vol. 114, no. 5, p. 641, 2014.